Release of serine/threonine-phosphorylated adaptors from signaling microclusters down-regulates T cell activation

Rémi Lasserre,[1,3] Céline Cuche,[1,3] Ronnie Blecher-Gonen,[4] Evgeny Libman,[4] Elise Biquand,[1,3] Anne Danckaert,[2] Deborah Yablonski,[4] Andrés Alcover,[1,3] and Vincenzo Di Bartolo[1,3]

[1]Lymphocyte Cell Biology Unit, Department of Immunology, and [2]Dynamic Imaging Platform, Imagopole, Institut Pasteur, F-75015 Paris, Cedex 15, France
[3]Centre National de la Recherche Scientifique, Unité de Recherche Associée 1961, F-75015 Paris, Cedex 15, France
[4]Rappaport Family Institute for Research in the Medical Sciences, The Ruth and Bruce Rappaport Faculty of Medicine, Technion-Israel Institute of Technology, IL-31096 Haifa, Israel

Antigen recognition within immunological synapses triggers and sustains T cell activation by nucleating protein microclusters that gather T cell receptors (TCRs), kinases, and adaptors. Dissipation of these microclusters results in signal termination, but how this process is regulated is unclear. In this paper, we reveal that release of the adaptors SLP76 and GADS from signaling microclusters is induced by the serine/threonine protein kinase HPK1 and that phosphorylation of GADS plays a major role in this process. We found that HPK1 was recruited into microclusters and triggered their dissipation by inducing the phosphorylation of a threonine-containing motif of GADS, together with the previously described serine phosphorylation of SLP76. These events induced the cooperative binding of 14-3-3 proteins to SLP76–GADS complexes, leading to their uncoupling from the transmembrane adaptor LAT and consequently reducing microcluster persistence and activation-induced gene transcription. These results demonstrate that serine/threonine phosphorylation of multiple TCR-proximal effectors controls the stability of signaling microclusters, thereby determining the intensity of T cell responses.

Introduction

Adaptive immune responses are initiated upon recognition by the T cell receptor (TCR) of peptide antigen–major histocompatibility complex complexes, displayed on the surface of antigen-presenting cells. TCR engagement induces a coordinated redistribution of receptors and signaling proteins at the immunological synapse, i.e., the interface between the T cell and the antigen-presenting cells (Monks et al., 1998; Grakoui et al., 1999). These events have been analyzed with high spatial and temporal resolution by imaging T cells activated on artificial stimulatory surfaces, such as coverslips coated with anti-CD3 antibodies (Bunnell et al., 2002) or lipid bilayers containing major histocompatibility complex–peptide complexes and adhesion molecules (Campi et al., 2005; Yokosuka et al., 2005). These approaches have revealed the assembly of submicrometer-scale protein complexes, or microclusters, containing the TCR and critical signaling molecules, including the protein kinases LCK and ZAP70, the adaptors SLP76, GADS, GRB-2, and LAT, and downstream effectors, such as VAV1, PLC-γ1, and Wiskott–Aldrich syndrome protein (Bunnell et al., 2002; Barda-Saad et al., 2004; Campi et al., 2005; Yokosuka et al., 2005; Carrizosa et al., 2009; Miletic et al., 2009). After T cell spreading over the stimulatory surface, TCR-containing microclusters enriched in activating kinases (e.g., LCK and ZAP70) and excluding negative regulators (e.g., the phosphatase CD45) preferentially form at the periphery of the immunological synapse. They then engage in centripetal movements toward the synapse center (Yokosuka et al., 2005; Varma et al., 2006). Microcluster components undergo different fates during this travel. TCRs accumulate at

Correspondence to Vincenzo Di Bartolo: vincenzo.di-bartolo@pasteur.fr

Abbreviations used in this paper: cSMAC, central supramolecular activation cluster; MBP, maltose-binding protein; NFAT, nuclear factor of activated T cell; PLA, proximity ligation assay; TCR, T cell receptor; TIRF, total internal reflection fluorescence; WT, wild type.

The Rockefeller University Press $30.00
J. Cell Biol. Vol. 195 No. 5 839–853
www.jcb.org/cgi/doi/10.1083/jcb.201103105

the center of the synapse forming the so-called central supramolecular activation cluster (cSMAC; Monks et al., 1998; Yokosuka et al., 2005) and are eventually down-regulated (Varma et al., 2006; Vardhana et al., 2010). On the other hand, molecules such as SLP76 and ZAP70 segregate from TCR microclusters before they reach the cSMAC (Bunnell et al., 2002; Yokosuka et al., 2005). Interestingly, reducing the mobility of microclusters toward the cSMAC by different means results in increased microcluster persistence and T cell activation (Mossman et al., 2005; Nguyen et al., 2008; Lasserre et al., 2010), suggesting that dynamic segregation of microcluster components reflects signal termination. Although ubiquitylation-mediated internalization/degradation of TCR subunits or other microcluster components has been implicated in signal inactivation (Balagopalan et al., 2007; Vardhana et al., 2010), the mechanisms triggering protein sorting from microclusters and signal termination are poorly characterized.

The cytoplasmic scaffold protein SLP76 plays a central role in TCR signal transduction and is indispensable for both thymocyte development and mature T cell activation (Koretzky et al., 2006). SLP76 is recruited into microclusters by binding to the transmembrane phosphoprotein LAT via the small adaptor GADS (Liu et al., 1999; Bunnell et al., 2006). The LAT–GADS–SLP76 complex is pivotal for signaling regulation and diversification because it coordinates the recruitment and activation of effectors belonging to several downstream pathways (Acuto et al., 2008). For instance, the association of SLP76 with the guanine nucleotide exchange factor VAV1, the adaptors NCK (Bubeck Wardenburg et al., 1998) and adhesion- and degranulation-promoting adaptor protein, (Peterson et al., 2001; Wang et al., 2009), the Tyr kinase Itk (Bunnell et al., 2000), and the Ser/Thr kinase HPK1 allows it to control actin cytoskeleton remodeling, cell adhesion, and gene transcription (Koretzky et al., 2006).

Recently, we have unveiled a negative feedback loop involving SLP76 that modulates T cell activation. HPK1 phosphorylates Ser376 of SLP76 and induces its interaction with members of the 14-3-3 protein family (Di Bartolo et al., 2007), ubiquitous molecules that regulate multiple cellular functions (Tzivion and Avruch, 2002). Biochemical and functional analyses suggested that binding of 14-3-3 to SLP76 down-modulates T cell signaling and activation (Di Bartolo et al., 2007), although the underlying mechanism remained uncharacterized. In support of our model, HPK1-deficient T cells showed increased signaling and responsiveness upon TCR stimulation (Shui et al., 2006).

Here, we demonstrate that HPK1 negatively regulates T cell activation by reducing the persistence of signaling microclusters and identify a threonine-containing motif in GADS whose phosphorylation plays a central role in this regulatory process. Our results indicate that HPK1-dependent phosphorylation of both GADS and SLP76 is required for the recruitment of 14-3-3 proteins. The resulting SLP76–GADS–14-3-3 complexes are released from LAT-containing microclusters and likely inactivated, thus down-modulating T cell activation. These data define a novel mechanistic link between Ser/Thr phosphorylation of TCR effectors, stability of signaling protein complexes, and down-regulation of T cell responses.

Results

HPK1 overexpression affects SLP76 microclusters

To address whether HPK1 may alter the formation and/or the dynamics of SLP76 signaling complexes, we analyzed SLP76-containing microclusters induced by immobilized stimulatory antibodies. SLP76-deficient J14 cells stably reconstituted with a YFP-tagged SLP76 fusion protein (J14-SLP76-YFP; Lasserre et al., 2010) were transiently transfected with a wild-type (WT) HPK1 construct fused to the red fluorescent protein mCherry (HPK1-mCherry). These cells were dropped on anti-CD3–coated coverslips, and protein microclusters were imaged in fixed cells after 3-min stimulation. Microclusters containing SLP76-YFP were detected in most untransfected cells, as expected, whereas their number was dramatically reduced in cells expressing HPK1-mCherry (Fig. 1 A). Conversely, transfection of an mCherry-labeled kinase-deficient mutant of HPK1 (HPK1-KD-mCherry) led to an increase in the number of SLP76 microclusters compared with control cells (Fig. 1 B), indicating that the impairment of SLP76 microclusters by HPK1 was dependent on its catalytic activity.

Interestingly, HPK1-KD-mCherry clearly accumulated in SLP76-containing microclusters (Fig. 1 B). Thus, we asked whether HPK1 recruitment into microclusters was a prerequisite for their negative regulation. Phosphorylation of Tyr379 of HPK1 has been shown to allow binding of this kinase to the SH2 domain of SLP76 (Sauer et al., 2001). Hence, we transfected an HPK1-mCherry construct bearing a Y379F mutation in J14-SLP76-YFP cells. As shown in Fig. 1 C, this mutant was not incorporated into microclusters nor affected their number, suggesting that Tyr379-dependent interaction of HPK1 with SLP76 is a critical step in down-regulating SLP76 microclusters. Thus, these data revealed that HPK1 regulates signaling microclusters and demonstrated that this function depends on HPK1 directly binding to SLP76 and catalytic activity.

HPK1 negatively regulates the persistence of SLP76-containing microclusters

To understand whether HPK1 overexpression prevents the formation of signaling microclusters and/or reduces their stability after initial assembly, J14-SLP76-YFP cells transfected with HPK1-mCherry constructs were stimulated on anti-CD3–coated coverslips and imaged in real time. In control cells expressing only endogenous HPK1, SLP76 microclusters appeared as soon as cells touched the stimulatory surface and could be observed for a few minutes after cells had completely spread (Fig. 2 A and Video 1, bottom cell) as previously described (Bunnell et al., 2002; Lasserre et al., 2010). Interestingly, in cells overexpressing HPK1-mCherry, microclusters formed as in control cells during spreading on the stimulatory surface, but they rapidly disappeared thereafter (Fig. 2 A and Video 1, top cell). Quantification of the lifetime of individual microclusters showed that overexpression of HPK1 significantly reduces their persistence compared with untransfected cells (Fig. 2 B). The rarity of microclusters in HPK1-overexpresing cells rendered the incorporation of HPK1-mCherry in SLP76 microclusters hard to detect

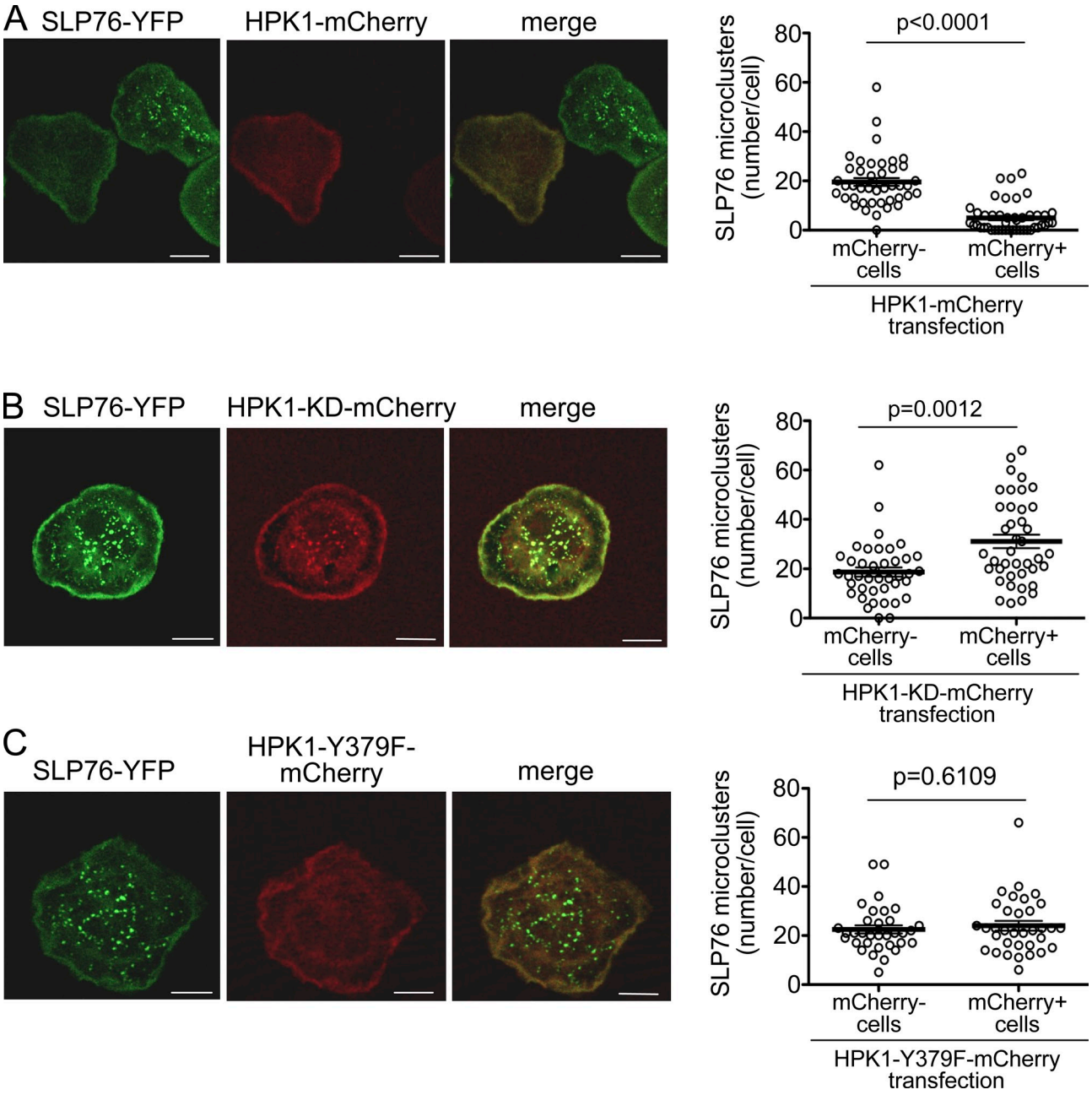

Figure 1. **HPK1 overexpression affects SLP76 microclusters.** (A) J14-SLP76-YFP cells were transfected with HPK1-mCherry. The day after transfection, cells were activated for 3 min on anti-CD3–coated coverslips, fixed, and analyzed by confocal microscopy. A single optical section at the level of the contact surface is shown. The plot shows the number of microclusters in cells expressing or not expressing the HPK1-mCherry construct. (B) J14-SLP76-YFP cells were transfected with HPK1-KD-mCherry and analyzed as in A. (C) J14-SLP76-YFP cells were transfected with HPK1-Y379F-mCherry and analyzed as in A. For all panels, images are representative of more than three independent experiments. Horizontal lines and error bars show means and SEM. Bars, 5 µm.

(Video 1). However, when visible, it was delayed as compared with microcluster formation. For instance, Fig. 2 C demonstrates that SLP76 incorporation increased for ∼40 s after microcluster detection, whereas HPK1-mCherry recruitment started to be detectable when the amount of SLP76 was at its maximum. Interestingly, the amount of SLP76 in microclusters started decreasing when HPK1 recruitment began, arguing that incorporation of HPK1 in SLP76 microclusters induces their dissipation.

Remarkably, continuous generation of new microclusters was detectable for some minutes in control cells but not in HPK1-mCherry transfectants after the extinction of the initial wave of microclusters accompanying cell spreading (Fig. 2 A and Video 1). This observation suggested that HPK1 not only promotes dissociation of SLP76 from existing complexes but also prevents its incorporation into new ones. Contrary to the WT construct, HPK1-KD-mCherry was incorporated into SLP76 microclusters and induced a significant increase in their mean lifetime (Fig. 2 B and Video 2), confirming that dissipation of SLP76 microclusters requires a catalytically active HPK1.

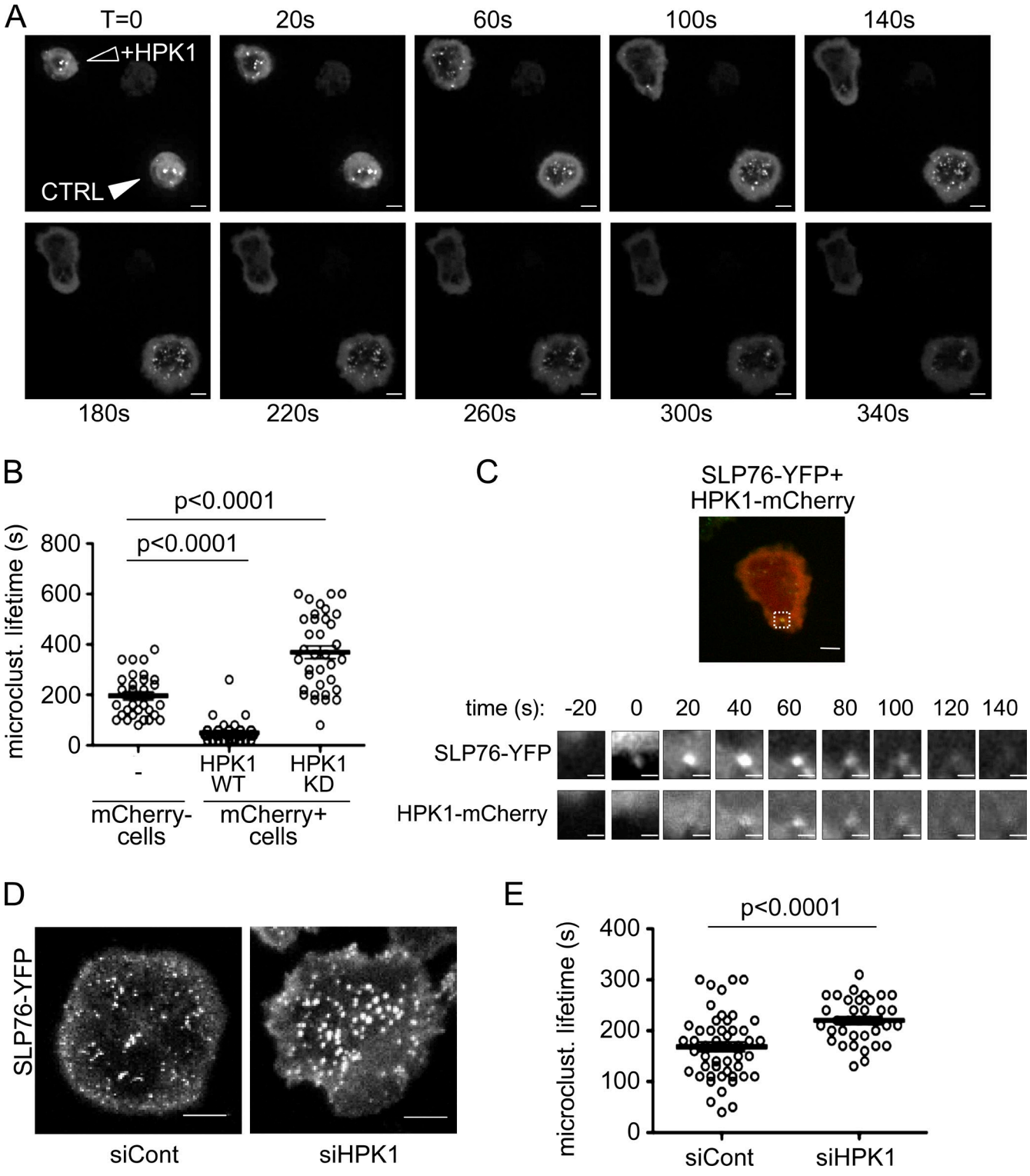

Figure 2. **HPK1 reduces the persistence of SLP76 microclusters.** (A) J14-SLP76-YFP cells transfected with HPK1-mCherry were activated on anti-CD3–coated coverslips and imaged with a spinning-disk confocal microscope at one image/20 s. Frames from Video 1 at different time points are shown. One untransfected control (CTRL) cell (closed arrowhead) and one cell expressing HPK1-mCherry (open arrowhead) are visible in each frame. (B). Lifetime of single SLP76-YFP microclusters was determined by manual tracking using time-lapse images of J14-SLP76-YFP cells, acquired as described in A. The plot shows SLP76 microcluster lifetime in untransfected cells and in cells expressing HPK1-mCherry or HPK1-KD-mCherry. (C, top) Z projection of the HPK1-mCherry–expressing cell shown in A, imaged after 80 s of activation. The boxed area highlights a microcluster containing both SLP76-YFP (green) and HPK1-mCherry (red). (bottom) Magnification of the boxed area shown in the top image at different time points. Time 0 corresponds to the first detection of this SLP76-YFP microcluster (i.e., 40 s in the time lapse displayed in A). Similar results were obtained in three independent experiments. (D) J14-SLP76-YFP cells transfected with control (siCont) or HPK1-specific (siHPK1) siRNAs were stimulated on anti-CD3 coverslips and analyzed as described in A. Knockdown efficiency was assessed by flow cytometry (Fig. S1). (E) SLP76 microcluster lifetime assessed in cells treated as in D. The plot shows pooled data of three experiments. Horizontal lines and error bars show means and SEM. Bars: (A, C [top], and D) 5 µm; (C, bottom) 1 µm.

We then addressed the role of endogenous HPK1 by analyzing the effect of HPK1 silencing on the persistence of SLP76 microclusters in live cells. SLP76-YFP–expressing cells were transfected with control or HPK1-specific siRNA oligonucleotides, typically yielding a knockdown efficiency of >70% (Fig. S1). Reduced HPK1 expression correlated with an increased lifetime of SLP76 microclusters (Fig. 2, D and E), similar to the effect of overexpressing HPK1-KD-mCherry (see previous paragraph and Fig. 2 B). It is noteworthy that changes in SLP76 expression were not detected upon overexpression or silencing of HPK1 (Fig. S1, B and C); hence, they cannot explain the observed effect on SLP76 microclusters.

The dynamics of SLP76 microclusters was also studied in cells stimulated by superantigen-pulsed primary dendritic cells. J14-SLP76-YFP cells transfected with control or HPK1-specific siRNAs were dropped on a monolayer of human dendritic cells, previously loaded with the bacterial superantigen SEE, and imaged in real time. Even in this setting, more closely reproducing physiological conditions, HPK1 knockdown appeared to extend the persistence of SLP76 microclusters as compared with control cells (Videos 3 and 4). Altogether, these results indicated that HPK1 plays a key role in controlling the persistence of SLP76 microclusters and limiting their generation upon sustained TCR stimulation.

HPK1 uncouples SLP76 from phospho-LAT microclusters

SLP76 is constitutively associated to the adaptor GADS and is recruited into microclusters via the inducible interaction of GADS with phosphorylated LAT. Thus, to dissect the mechanism underlying the HPK1-induced dissipation of SLP76 microclusters, we compared the effect of HPK1 silencing on the number of SLP76 and phospho-LAT microclusters. J14-SLP76-YFP cells were transfected with control or HPK1-targeting siRNAs, stimulated on anti-CD3–coated coverslips, and stained with phosphospecific antibodies against Tyr191 of LAT. SLP76 microclusters were comparable in numbers in HPK1-silenced and control cells for ≤2 min of stimulation (Fig. S2 A). However, they were significantly more abundant in HPK1 knockdown than in control cells at 3 min of stimulation and later (Fig. 3, A and B). On the other hand, phospho-LAT microclusters were not affected by HPK1 knockdown for ≤3 min, whereas their number declined thereafter with a delayed kinetics in HPK1-silenced compared with control cells (Fig. 3, A and C). A similar delay between SLP76 and LAT microcluster down-regulation was observed in primary human T cells transfected with HPK1-specific siRNAs. Higher numbers of phospho-SLP76 microclusters were detected in HPK1 knockdown cells at 3 and 5 min of stimulation compared with control cells (Fig. 3, D and E), whereas phospho-LAT microclusters were slightly affected only at 5 min (Fig. 3 F). Mean HPK1 knockdown efficiency in these cells was ∼60% (Fig. S2 B).

Consistent with these results, transfection of J14-SLP76-YFP cells with HPK1-mCherry led to a significant reduction in the number of SLP76 microclusters compared with control cells but had no significant effect on phospho-LAT microclusters in cells stimulated for 3 min (Fig. S2, C and D). Collectively, these data indicated that the primary role of HPK1 is to regulate clustering of SLP76, although it may exert some delayed effect on phospho-LAT microclusters.

Further insight into the mechanism by which HPK1 affects SLP76 microclusters was obtained by analyzing SLP76-associated proteins by coimmunoprecipitation in cells stably expressing a FLAG-SLP76 construct (J14-SLP76-WT; Di Bartolo et al., 2007). HPK1 silencing increased the amount of LAT coprecipitating with SLP76 in anti-CD3–stimulated cells, whereas the amount of coprecipitating GADS was unaffected (Fig. 3 G, compare bottom and middle). Efficient HPK1 silencing and impaired phosphorylation of its substrate Ser376 were confirmed by Western blotting (Fig. S3 A). Conversely, transient cotransfection of HPK1 with FLAG-SLP76 in J14 cells impaired the activation-induced coprecipitation of LAT but not GADS with FLAG-SLP76 at 5 min of stimulation (Fig. 3 G), although LAT phosphorylation was not affected (Fig. S3 B). Together, these results demonstrated that HPK1 controls the persistence of SLP76 microclusters by uncoupling SLP76–GADS complexes from phosphorylated LAT.

Persistence of SLP76 microclusters is partially dependent on HPK1-induced binding of 14-3-3 proteins to SLP76

Because we previously showed that HPK1 phosphorylates Ser376 of SLP76 and induces its binding to 14-3-3 proteins (Di Bartolo et al., 2007), we probed the involvement of these events in the dissipation of SLP76 microclusters. First, we compared the distribution of SLP76 microclusters and SLP76–14-3-3ζ complexes in SLP76-YFP–expressing cells. SLP76–14-3-3ζ complexes were specifically detected in activated cells by using an in situ proximity ligation assay (PLA; Fig. S4, A and B; see Materials and methods and Söderberg et al., 2006) but appeared to be segregated from SLP76-YFP microclusters (Fig. 4 A, top). Although the latter were adjacent to the cell–coverslip interface, SLP76–14-3-3ζ complexes were mostly far from this region (Fig. 4 A, bottom). Accordingly, only SLP76 microclusters, which are localized in close proximity of the plasma membrane, could be detected by total internal reflection fluorescence (TIRF) microscopy, whereas SLP76–14-3-3ζ complexes were visible only by epifluorescence (Fig. S4 C). These data strongly suggest that 14-3-3ζ binding to SLP76 and retention of SLP76 in microclusters are mutually exclusive.

Additionally, the number of microclusters was significantly increased in cells expressing a YFP-labeled SLP76-S376A mutant, which cannot bind 14-3-3 proteins (Fig. 4 B). This result, implicating the SLP76–14-3-3 interaction in the regulation of SLP76 microclusters, was reminiscent of the effect of HPK1 knockdown (Fig. 3). However, the latter produced larger effects than SLP76-S376A-YFP expression (∼63 vs. 29% increase in microclusters compared with control cells, respectively, at 3 min of stimulation; compare Figs. 3 C and 4 B), suggesting that HPK1 may exert additional effects on these signaling complexes.

Based on the propensity of 14-3-3 proteins to form homo- or heterodimers simultaneously binding two phosphorylated motifs (Tzivion and Avruch, 2002), we hypothesized that HPK1 might generate a second 14-3-3 binding site in SLP76 or in an associated protein, stabilizing the interaction with Ser376. Hence, we probed SLP76-associated proteins, isolated from

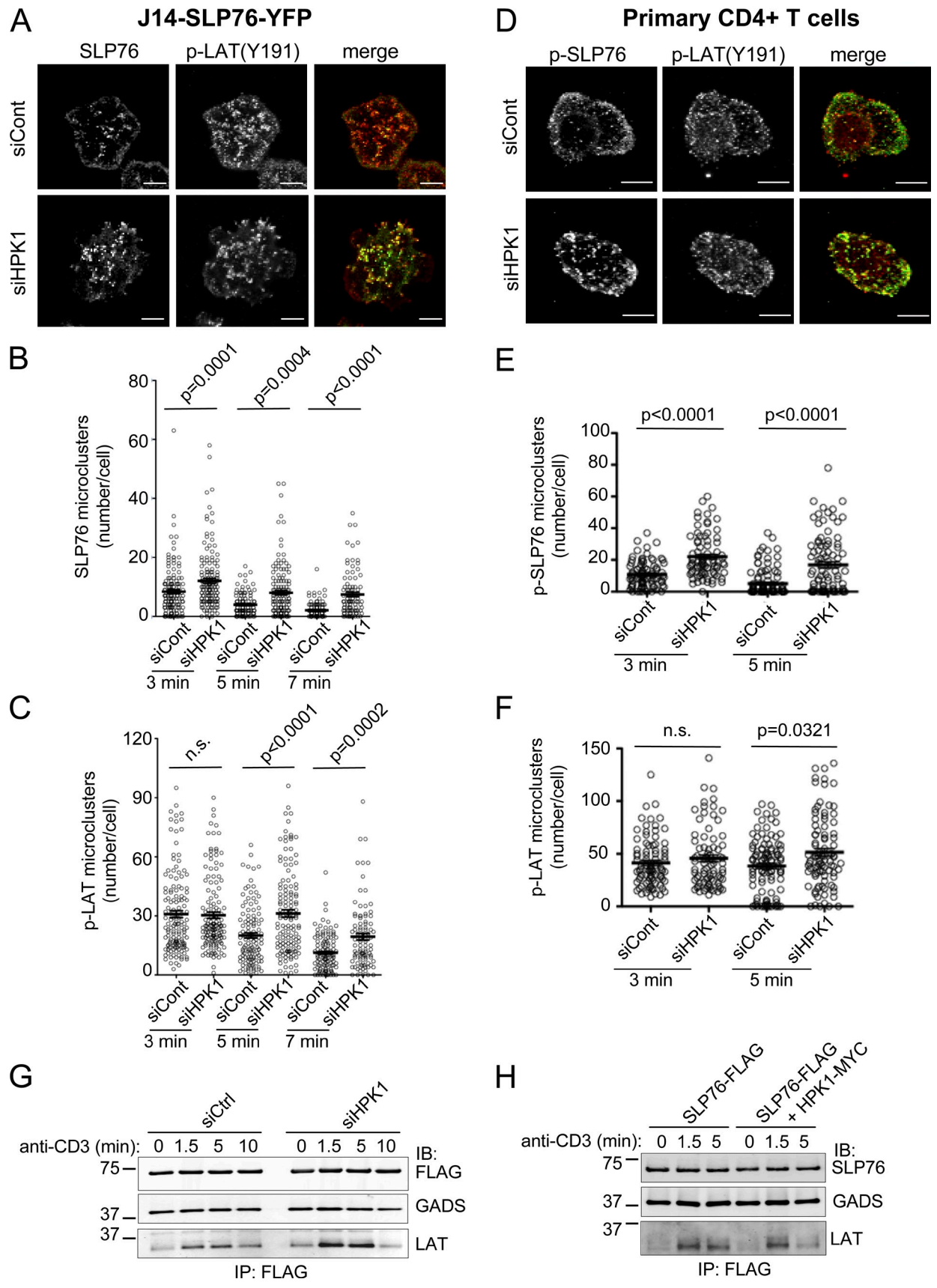

Figure 3. **HPK1 uncouples SLP76 from LAT microclusters.** (A) J14-SLP76-YFP cells transfected with control (siCont) or HPK1-specific (siHPK1) siRNAs were activated for 3 min on anti-CD3–coated coverslips, fixed, stained with antiphospho-LAT (Y191) mAbs, and imaged by confocal microscopy. Results are representative of three independent experiments. (B and C) J14 cells expressing SLP76-YFP were transfected as in A and stimulated for the indicated time

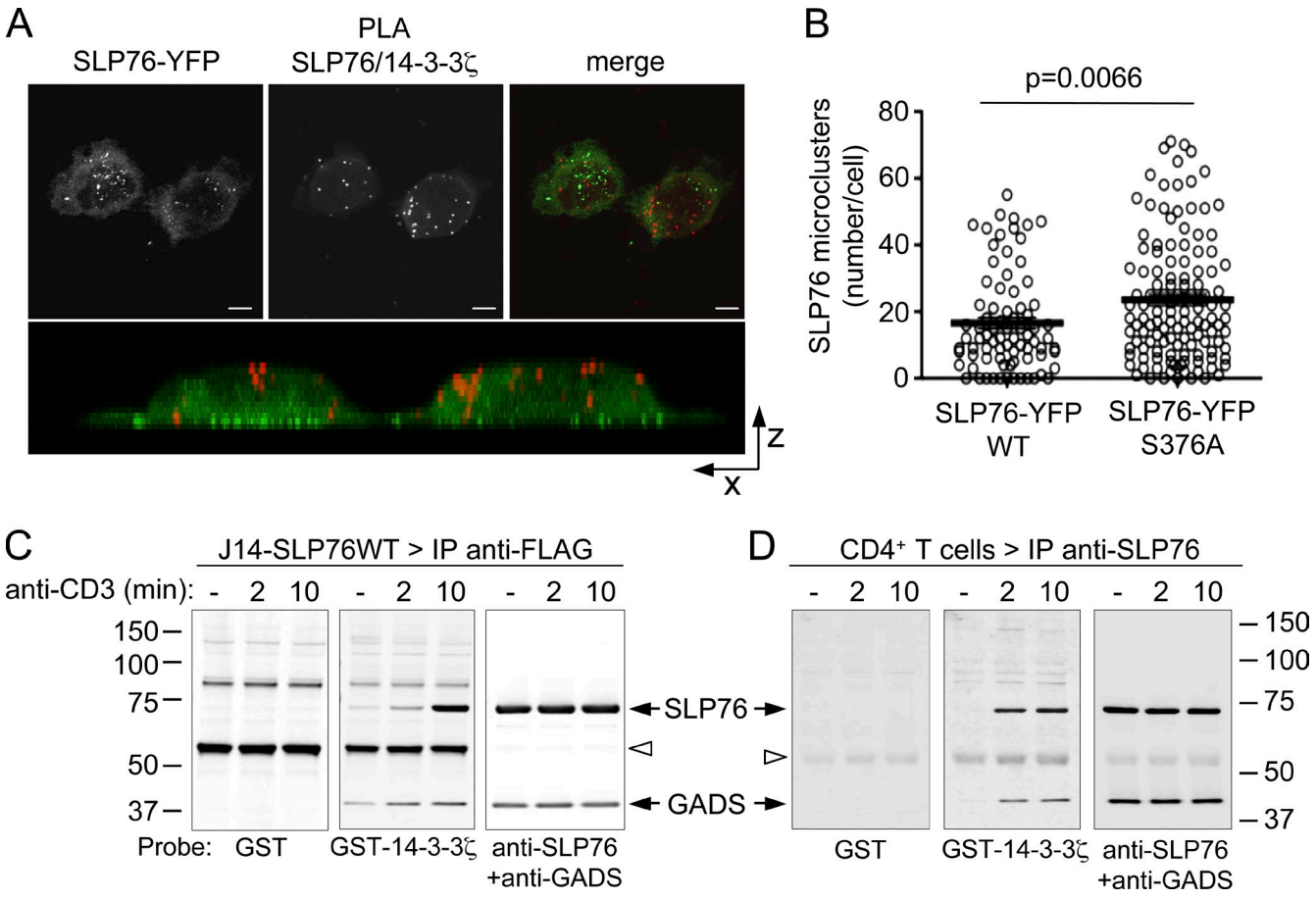

Figure 4. **Persistence of SLP76 microclusters is partially dependent on 14-3-3 proteins binding to phosphorylated Ser376.** (A) J14-SLP76-YFP cells were activated for 3 min on anti-CD3–coated coverslips, fixed, and stained with anti-SLP76 and anti–14-3-3ζ antibodies. SLP76-YFP microclusters (left; green in right image) and SLP76–14-3-3ζ complexes detected by in situ PLA (middle; red in right image) were visualized by confocal microscopy. A z-stack projection is shown. Bottom image represents an x-z projection of the cells shown in top images. Images are representative of three independent experiments. Bars, 5 µm. (B) J14 cells were transiently transfected with SLP76-YFP-WT or -S376A constructs. Cells were activated as in A, fixed, and imaged by confocal microscopy. SLP76-YFP microclusters were automatically counted (see Materials and methods) in cells expressing comparable levels of YFP labeling. Horizontal lines and error bars show means and SEM. (C) J14-SLP76-WT cells stably expressing FLAG-SLP76 were stimulated with anti-CD3 mAbs for the indicated time points, lysed, and immunoprecipitated (IP) with anti-FLAG mAbs. Samples were sequentially analyzed by GST (left) and GST–14-3-3ζ (middle) overlay assays followed by immunoblotting with anti-SLP76 and anti-GADS antibodies (right). Similar results were obtained in four independent experiments. Open arrowheads indicate heavy chains of precipitating antibodies. Mobility of molecular mass markers (in kilodaltons) is shown on the left. (D) Human CD4+ T cells were treated as in C, immunoprecipitated with anti-SLP76 antibodies, and subjected to overlay assays and immunoblotting as in C. This result is representative of two independent experiments. Mobility of molecular mass markers is shown on the right in kilodaltons.

J14-SLP76-WT cells, with a GST–14-3-3ζ fusion protein in an overlay assay. In addition to SLP76, a protein of ∼40 kD was bound by GST–14-3-3ζ but not by GST (Fig. 4 C, middle and left). This interaction was detectable in unstimulated cells and was increased after stimulation. Immunoblotting identified this protein as GADS (Fig. 4 C, right). Similar results were obtained when the GST–14-3-3ζ overlay assay was performed on SLP76 immunoprecipitates from human CD4+ T cells (Fig. 4 D). These results identified GADS as a novel 14-3-3–interacting protein and suggested its potential involvement in mediating HPK1 regulation of signaling microclusters.

HPK1 phosphorylates GADS and regulates its interaction with 14-3-3 proteins

The aforementioned results prompted us to ask whether HPK1 may regulate 14-3-3 binding to GADS. First, we used an in vitro

points. SLP76-YFP (B) and phospho-LAT (p-LAT; C) microclusters were imaged and automatically counted (see Materials and methods). Circles represent the number of microclusters/cell of pooled data from three independent experiments. (D) Human primary CD4+ T cells, transfected with control or HPK1-specific siRNAs, were activated as in A, fixed, and stained with antiphospho-SLP76 (Y128) and antiphospho-LAT (Y191) mAbs. Images were acquired as in A. HPK1 knockdown efficiency was assessed by flow cytometry (Fig. S2 B). (E and F) Human primary CD4+ T cells were transfected and stimulated as in D and fixed at the indicated time points. Phospho-SLP76 (p-SLP76) and phospho-LAT microclusters were counted as in B. (G) J14-SLP76-WT cells expressing FLAG-SLP76 and transfected with control or HPK1-specific siRNAs were stimulated by anti-CD3 antibodies for the indicated time points, lysed, and immunoprecipitated (IP) by the anti-FLAG mAb. Proteins were separated by electrophoresis in nonreducing conditions and analyzed by immunoblotting (IB) as indicated. Comparable results have been obtained in two independent experiments. See Fig. S3 A for analysis of HPK1 knockdown efficiency. (H) J14 cells transiently transfected with SLP76-FLAG and/or HPK1-MYC constructs were stimulated for the indicated time points, lysed, and immunoprecipitated by anti-FLAG antibodies. Proteins were analyzed by immunoblotting as in G. Mobility of molecular mass markers (in kilodaltons) is shown on the left. Horizontal lines and error bars show means and SEM. Bars, 5 µm.

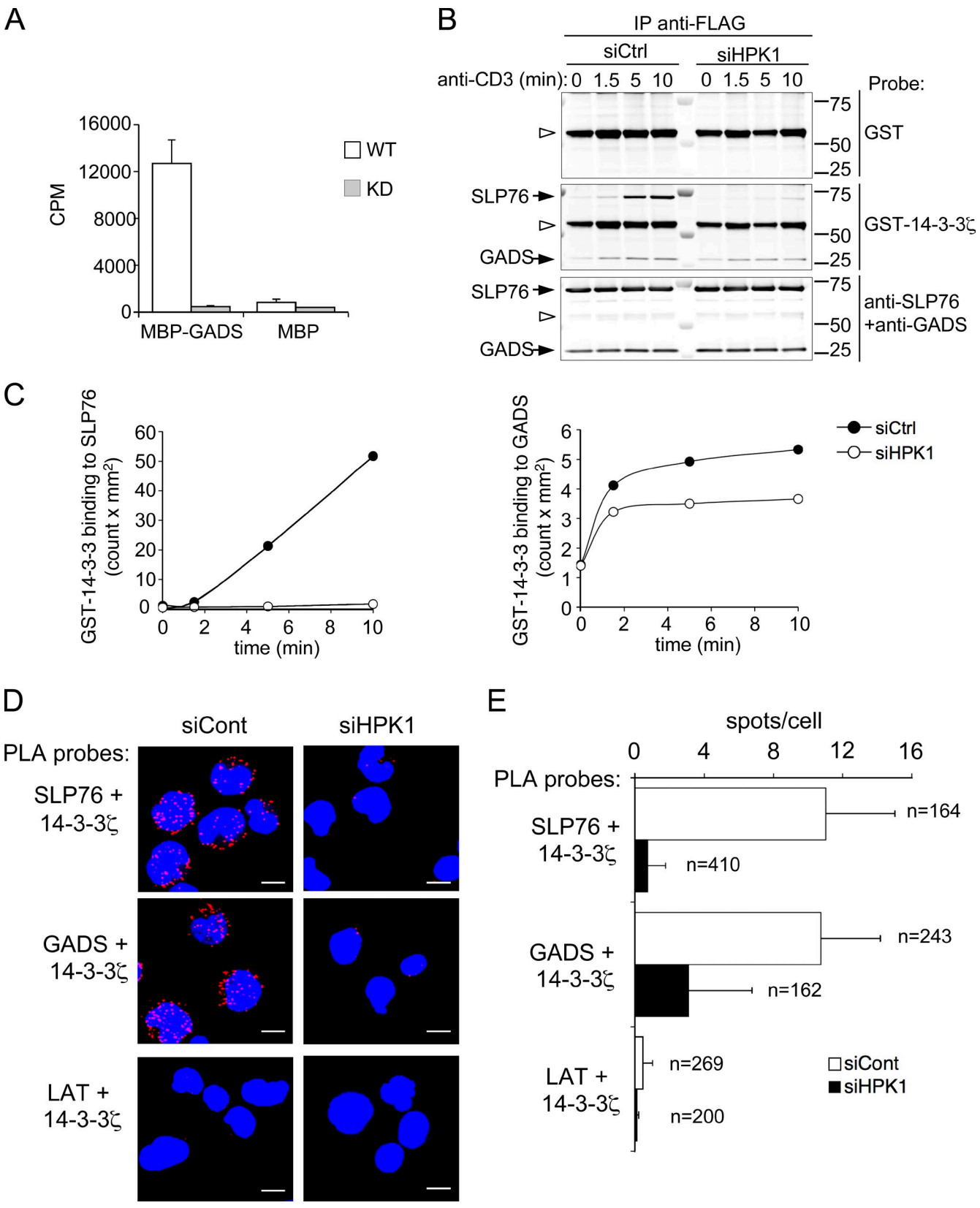

Figure 5. **HPK1-dependent binding of 14-3-3ζ to GADS.** (A) HPK1-HA constructs, wild type (WT) or kinase deficient (KD), were transfected in COS7 cells and immunoprecipitated (IP) with anti-HA mAbs. Recombinant MBP or MBP-GADS was added to either sample and incubated with [^{32}P]ATP. Supernatants were then spotted onto Whatman filters, and incorporated radioactivity was measured. Comparable results have been obtained in three independent experiments. Error bars indicate SDs of triplicates. (B) J14-SLP76-WT cells expressing FLAG-SLP76 and transfected with control (siCont) or HPK1-specific (siHPK1) siRNAs were stimulated by anti-CD3 mAbs for the indicated time points, lysed, and immunoprecipitated with anti-FLAG mAbs. Samples were analyzed by GST (top) and GST–14-3-3ζ (middle) overlay assay followed by Western blotting with anti-SLP76 and anti-GADS antibodies (bottom).

kinase assay to test whether GADS is a substrate of HPK1. Immunoprecipitated WT or kinase-deficient HPK1 was incubated with maltose-binding protein (MBP) or an MBP-GADS fusion protein in the presence of [^{32}P]ATP. A significant incorporation of ^{32}P over background was observed when MBP-GADS was incubated with WT HPK1 but not with the kinase-deficient construct (Fig. 5 A).

We then asked whether HPK1 regulates the interaction of 14-3-3ζ with GADS. We transfected J14-SLP76-WT cells with control or HPK1-specific siRNAs and immunoprecipitated FLAG-SLP76 and associated proteins. Efficient HPK1 knockdown (Fig. S3 C) almost completely inhibited of GST–14-3-3ζ binding to FLAG-SLP76 in an overlay assay (Fig. 5, B [middle] and C [left]). Maximum binding of GST–14-3-3ζ to GADS was reduced by ∼50% in HPK1 knockdown cells compared with control cells (Fig. 5, B [middle] and C [right]). Although the inhibition of GST–14-3-3ζ binding to GADS in this assay was not complete, this result indicated a role of HPK1 in inducing 14-3-3 binding to GADS.

Finally, we probed the role of HPK1 in regulating the interaction of 14-3-3ζ with GADS in intact cells. Jurkat cells, transfected with control or HPK1-specific siRNAs, were stimulated on anti-CD3–coated coverslips and analyzed by in situ PLA with different antibody combinations. Labeling with anti-SLP76 and anti–14-3-3ζ antibodies yielded a positive PLA signal that was abolished upon HPK1 silencing (Fig. 5, D [top] and E), confirming that SLP76 binding to 14-3-3ζ is induced by HPK1 (Di Bartolo et al., 2007). Staining with anti-GADS and anti–14-3-3ζ antibodies also yielded a strong PLA signal in control cells, validating the interaction between these proteins, which was impaired by HPK1 silencing (Fig. 5, D [middle] and E). Conversely, no detectable PLA signal was observed after staining with anti-LAT and anti–14-3-3ζ antibodies (Fig. 5, D [bottom] and E). Collectively, these data demonstrated that HPK1 controls the interaction of 14-3-3 proteins with GADS.

14-3-3ζ binds a phosphothreonine-containing motif of GADS

Because 14-3-3 protein binding to their target is usually induced by Ser/Thr phosphorylation of conserved motifs (Tzivion and Avruch, 2002), we inspected the human GADS sequence in search of potential 14-3-3 binding sites. We identified a conserved RRHTDP sequence, resembling a type I 14-3-3 binding motif (RXXp(S/T)XP; Johnson et al., 2010), encompassing Thr262 (Thr254 in murine GADS). Interestingly, this residue was previously reported to be phosphorylated in T cells (Salomon et al., 2003; Brill et al., 2004), and a similar motif in the adaptor Gab2 (RRNpTLP) was previously shown to bind 14-3-3 proteins (Brummer et al., 2008). Hence, we mutated Thr254 to Ala in a murine GADS construct fused to the CFP (CFP-GADS; Bunnell et al., 2006) and tested the ability of this mutant to bind 14-3-3ζ. J14 cells were transfected with FLAG-SLP76 alone or together with WT or mutant CFP-GADS. Analysis of anti-FLAG immunoprecipitates by an overlay assay revealed that GST–14-3-3ζ bound in an inducible manner to FLAG-SLP76 and endogenous GADS as well as to transfected CFP-GADS (Fig. 6 A, top). Conversely, binding of GST–14-3-3ζ to CFP-GADS-T254A was almost undetectable (Fig. 6 A, top). Moreover, an antibody raised against phosphorylated RRXp(S/T) motifs detected CFP-GADS in a stimulation-dependent manner (Fig. 6 A, middle) but not CFP-GADS-T254A, confirming that Thr254 is phosphorylated in vivo and demonstrating a causal link between Thr254 phosphorylation and GST–14-3-3ζ binding to GADS.

To assess the relative contribution of SLP76 and GADS binding sites to 14-3-3 recruitment, J14 cells were transfected with FLAG-SLP76 and CFP-GADS constructs, either WT or mutant, in various combinations. Immunoblotting on SLP76 immunoprecipitates showed that GADS-T254A mutation reduced the coprecipitation of 14-3-3ζ more strongly than the SLP76-S376A mutation (Fig. 6 B, bottom). Expression of both mutants further reduced 14-3-3ζ binding (Fig. 6 B, bottom), demonstrating that stable interaction of 14-3-3ζ with the SLP76–GADS complex depends on both Ser376 and Thr254. Importantly, neither mutation altered the constitutive SLP76–GADS interaction (Fig. 6 B, top and middle). These data identified Thr254 of GADS as a 14-3-3 binding site and highlighted its prominent role in regulating the association of 14-3-3 proteins to SLP76–GADS complexes.

14-3-3 binding to SLP76 and GADS cooperatively affects microcluster stability and T cell activation

Based on the aforementioned observations, we aimed to correlate 14-3-3 binding to SLP76 and GADS with microcluster stability and T cell activation. First, we analyzed the persistence of SLP76 microclusters in cells expressing various SLP76-YFP and CFP-GADS constructs stimulated on anti-CD3–coated coverslips for 5 min. The number of SLP76 microclusters was significantly increased in cells expressing the CFP-GADS-T254A compared with those transfected with CFP-GADS (Fig. 7 A). Expression of YFP-SLP76-S376A also increased the number of microclusters compared with YFP-SLP76–expressing cells, although it was less effective than CFP-GADS-T254A (Fig. 7 A). Simultaneous expression of both mutants further increased the number of microclusters as compared with either mutant alone (Fig. 7 A). Of note, phospho-LAT microclusters

Similar results have been obtained in three independent experiments. Open arrowheads indicate heavy chains of the precipitating antibodies. HPK1 knockdown efficiency was assessed by immunoblotting (Fig. S1 C). Mobility of molecular mass markers is shown on the right in kilodaltons. (C) Quantification of GST–14-3-3ζ binding to SLP76 (left) and GADS (right) in overlay assays shown in B. Bands in B (middle and bottom) were acquired and quantified as outlined in Materials and methods. Intensity of bound GST–14-3-3ζ bands was normalized by the relative amount of SLP76 (left) or GADS (right) in the same lane. (D) Jurkat cells transfected with control or HPK1-specific siRNAs were activated for 10 min on anti-CD3–coated coverslips, fixed, and stained with the antibody pairs indicated on the left and by DAPI for visualizing nuclei (blue). Protein complexes (red) were detected by in situ PLA. A z-stack projection is shown in each image. Bars, 5 µm. (E) Images obtained by in situ PLA experiments as shown in D were analyzed using the BlobFinder software to automatically count spots generated by protein–protein interactions. Histograms show means and SEM of the number of spots per cell from two independent experiments. The number of cells analyzed is indicated beside each bar.

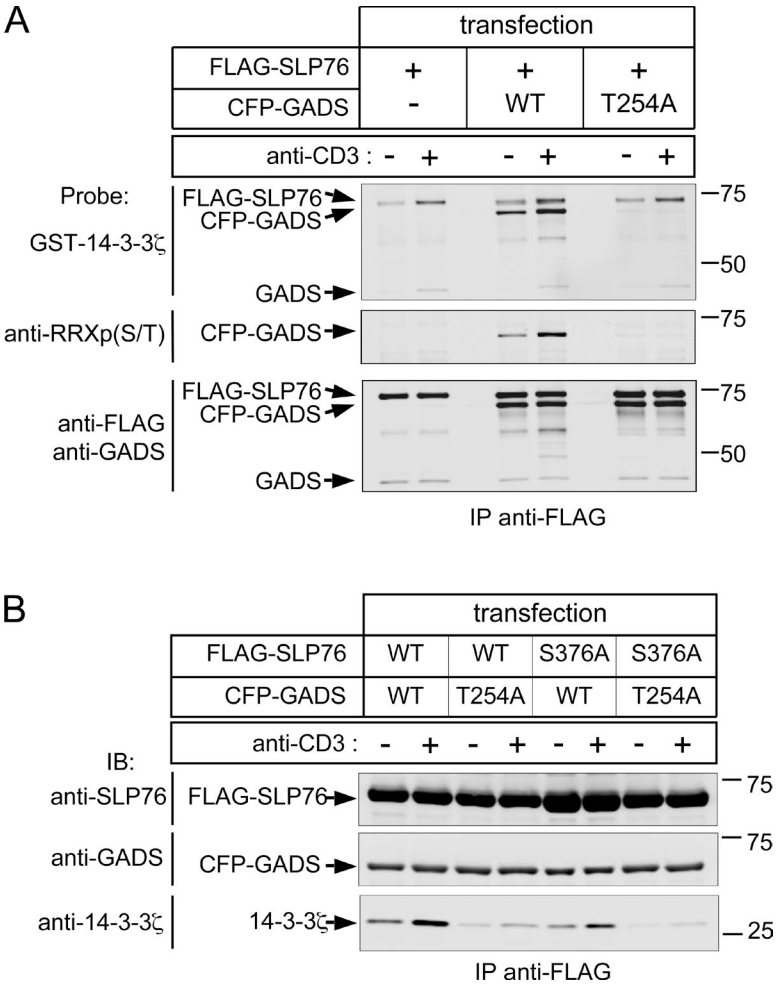

Figure 6. **Mutation of Thr254 impairs 14-3-3ζ binding to GADS and coprecipitation with the SLP76–GADS complex.** (A) J14 cells were transiently transfected with FLAG-SLP76 together with CFP-GADS constructs, either wild type (WT) or T254A. Cells were stimulated (+) or not stimulated (−) with anti-CD3 mAbs, immunoprecipitated (IP) with anti-FLAG antibodies, and analyzed by GST–14-3-3ζ overlay assay (top) followed by immunoblotting (IB) with the antiphospho-RRXS/T motif (middle) and anti-FLAG plus anti-GADS mAbs (bottom). (B) J14 cells were transiently transfected with FLAG-SLP76-WT or -S376A together with either CFP-GADS-WT or CFP-GADS-T254A. Cells were treated as in A, immunoprecipitated with anti-FLAG antibodies, and then analyzed by immunoblotting with anti-SLP76 (top), anti-GADS (middle), and 14-3-3ζ antibodies (bottom). For both panels, data are representative of two independent experiments giving similar results. Mobility of molecular mass markers (in kilodaltons) is shown on the right.

were also increased at this time point by SLP76 and GADS mutations (Fig. S5 A), indicating that alterations of these two adaptors indirectly affect LAT clustering.

Finally, we evaluated the functional response of T cells expressing SLP76 and GADS mutants by measuring the activation of the nuclear factor of activated T cell (NFAT) transcription factor. J14-SLP76-WT and -S376A cell lines expressing FLAG-tagged WT SLP76 or the S376A mutant (Di Bartolo et al., 2007) were transfected with CFP-GADS or CFP-GADS-T254A expression vector, together with an NFAT-luciferase reporter plasmid. Measurement of luciferase activity in cells stimulated with anti-CD3 and anti-CD28 antibodies showed that overexpressing CFP-GADS-T254A in J14-SLP76-WT cells led to higher NFAT activation than CFP-GADS transfection (Fig. 7 B). J14-SLP76-S376A cells expressing CFP-GADS also showed higher NFAT activity compared with J14-SLP76-WT transfected with this construct. Moreover, expression of CFP-GADS-T254A in J14-SLP76-S376A further increased NFAT activity (Fig. 7 B), indicating that simultaneous mutation of both 14-3-3 binding sites resulted in the highest T cell activation. Comparable expression of all constructs was verified by immunoblotting (Fig. S5 B). Altogether, these results indicated that the simultaneous interaction of 14-3-3 to SLP76 and GADS negatively regulates the stability of signaling complexes and functional activation of T cells.

Discussion

This work shows for the first time that HPK1 modulates TCR-proximal signaling and T cell activation by regulating the stability of critical protein complexes at the immunological synapse. We found that the persistence of SLP76 microclusters induced by TCR stimulation is dependent on HPK1 activity. HPK1 incorporation into SLP76 microclusters coincides with their rapid dissipation caused by a 14-3-3–mediated uncoupling of SLP76–GADS complexes from LAT. Persistence of phospho-LAT microclusters appears also affected by HPK1 but with some delay compared with SLP76 microclusters. These kinetic differences suggest that the effect on phospho-LAT clustering is consequent to the release of the SLP76–GADS complex, possibly because of the loss of stabilizing protein–protein interactions dependent on SLP76 and/or GADS. In support of the hypothesis that HPK1 does not target LAT directly, phospho-LAT microclusters are increased when 14-3-3 binding to SLP76 and GADS is impaired (Fig. S5 A). Collectively, these results show that a major function of HPK1 is to uncouple the SLP76–GADS from phosphorylated LAT, leading to negative regulation of T cell activation.

The results described here reveal that the mechanism of HPK1-dependent tuning of TCR-proximal signaling is more complex than initially reported because it involves a previously unidentified 14-3-3 binding site in GADS in addition to Ser376

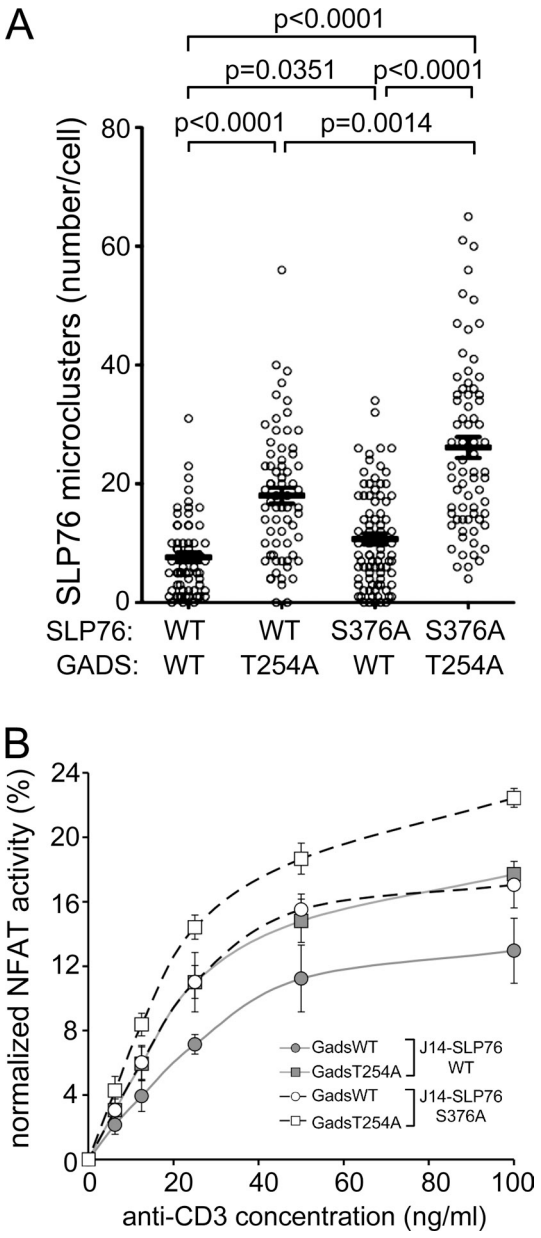

Figure 7. **Mutation of 14-3-3ζ binding sites of SLP76 and GADS leads to additive increase in SLP76 microclusters and NFAT activation.** (A) J14 cells were transiently transfected with SLP76-YFP, -WT, or -S376A together with CFP-GADS constructs, either WT or a T254A mutant. Cells were stimulated for 5 min on anti-CD3–coated coverslips, fixed, and imaged by confocal microscopy. The number of SLP76 microclusters was automatically assessed in selected cells showing homogeneous levels of YFP and CFP fluorescence. A similar analysis was performed on phospho-LAT microclusters (Fig. S5 A). Horizontal lines and error bars show means and SEM. (B) J14 cells stably expressing FLAG-SLP76 (J14-WT) or FLAG-SLP76-S376A (J14-S376A) were transiently cotransfected with the indicated CFP-GADS construct and an NFAT-luciferase reporter plasmid. Cells were stimulated with the indicated concentrations of plate-bound anti-CD3 and 1 µg/ml of soluble anti-CD28 mAbs for 5 h. Control samples were stimulated with PMA and Ca^{2+} ionophore to assess maximal NFAT-dependent transcription. Luciferase activity was measured in cell lysates. Data represent means ± SD of normalized luciferase activity from quadruplicate samples expressed as a percentage of maximal luciferase activity. Comparable expression levels of all constructs are shown in Fig. S5 B.

of SLP76 (Di Bartolo et al., 2007). Thr254 in murine GADS (corresponding to Thr262 in the human protein) was necessary for 14-3-3 binding and for negative regulation of microcluster stability and T cell activation. Moreover, disruption of this 14-3-3 binding site had a stronger impact on SLP76 microcluster persistence than mutation of Ser376, possibly because binding of 14-3-3 to GADS disturbs the interaction of the SH2 domain of GADS with phospho-LAT, either by steric hindrance or by inducing a conformational change. However, simultaneous mutation of both Ser376 and Thr254 had additive effects on both persistence of SLP76 microclusters and NFAT transcriptional activity upon T cell stimulation, suggesting a cooperative stabilization of the interaction of 14-3-3 with the SLP76–GADS complex. This finding is consistent with 14-3-3 proteins forming homo- and heterodimers that usually require interaction with two phosphorylation sites for stable binding (Tzivion and Avruch, 2002). Based on these results, we propose a model whereby recruitment of HPK1 in SLP76-containing microclusters leads to phosphorylation of both SLP76 and GADS on Ser376 and Thr262, respectively. These posttranslational modifications enable recruitment of a 14-3-3 protein dimer, which in turn enforces dissociation of the SLP76–GADS–14-3-3 complex from phospho-LAT and consequently down-regulates TCR-induced signal transduction (Fig. 8).

The subsequent fate of the pool of SLP76 (and GADS) released from microclusters is unknown yet. Although a fraction of it could still be signaling competent because of its interaction with other effectors (Bunnell et al., 2006), the correlation between removal from microclusters and reduced T cell activation reported here rather hints at an inactivation process. Hence, 14-3-3–bound SLP76 might be sorted for degradation or recycling. We could not detect significant changes in the total amount of SLP76 during the stimulation time analyzed (10 min), but we cannot exclude that degradation occurs later. Reincorporation of SLP76 into new microclusters has been previously described by others (Barr et al., 2006), but according to our model, it would imply release of 14-3-3 and dephosphorylation of Ser376. However, we found that both Ser376 phosphorylation and 14-3-3 binding to SLP76 were long lasting (i.e., 45–60 min; Di Bartolo et al., 2007) and that no additional microclusters were generated after the extinction of the first wave accompanying cell spreading on anti-CD3 coverslips in cells overexpressing HPK1 (Fig. 2 A and Video 1). Both observations argue against a recycling of released SLP76; hence, further studies are required to address these issues.

Intriguingly, HPK1 knockdown more potently impaired GST–14-3-3ζ binding to SLP76 than to GADS in the overlay and in situ PLA assays, whereas direct mutation of the 14-3-3 binding site in GADS had stronger effects on 14-3-3ζ coprecipitation and on microcluster stability than mutation in SLP76. The reason for this difference is unknown and may depend, in part, on the different assay used. However, although HPK1 phosphorylates GADS in vitro, they do not allow us to exclude the existence of redundant kinases that may replace HPK1 in phosphorylating GADS in vivo.

The effect of HPK1 on microcluster persistence is reminiscent of that previously described for the ubiquitin E3

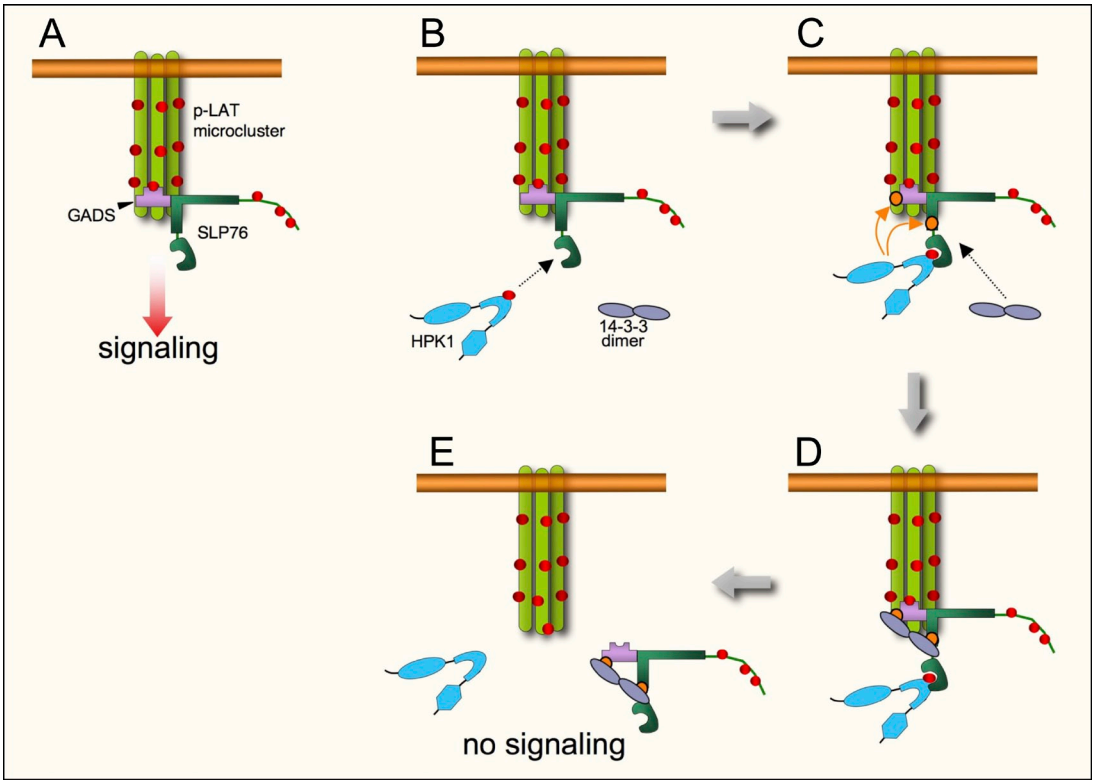

Figure 8. **Model of regulation of microcluster persistence and signaling by HPK1.** (A) SLP76–GADS complexes (only one is depicted for clarity) are recruited to the phosphorylated transmembrane adaptor LAT to form signaling-competent microclusters. (B and C) When phosphorylated on Tyr379, HPK1 is incorporated into microclusters by interacting with the SH2 domain of SLP76 (B) and phosphorylates Ser376 of SLP76 and Thr262 of GADS (C). (D and E) 14-3-3 proteins then bind to SLP76–GADS complexes through these phosphorylated residues (D), thus leading to dissociation of these complexes from phospho-LAT (p-LAT) and terminating signaling (E).

ligase c-Cbl (Balagopalan et al., 2007). Indeed, c-Cbl incorporation into LAT- and SLP76-containing microclusters induces their dissipation, although the mechanisms allowing c-Cbl–dependent control of microcluster stability remain to be identified (Balagopalan et al., 2007, 2011). Therefore, HPK1 and c-Cbl appear to modulate microcluster persistence, likely by different mechanisms, suggesting that multiple negative feedback loops operate to control protein clustering at immunological synapses. This also implies that the dissipation of signaling protein complexes is not only dictated by "passive" mechanisms, e.g., stochastic release of SH2-mediated interactions followed by dephosphorylation of critical tyrosine residues, but also by specific mechanisms "actively" driving the dissociation of key components.

Tuning of T cell signaling by HPK1 might be regulated in an activation- and/or differentiation-dependent fashion. Indeed, it has been shown that the expression of HPK1 in stimulated T cells is first up-regulated and then decreased because of caspase-dependent cleavage. Such modulation appears to control the activation of the NFκB pathway, thus inducing a change in T cell sensitivity to activation-induced apoptosis (Brenner et al., 2005), but it may also affect upstream signaling events. If this is the case, the regulatory mechanism described here would be active in naive but not in previously activated cells.

TCR-independent stimuli may also tune HPK1 activity and, consequently, T cell responsiveness. For instance, it has been proposed that secretion of prostaglandin E2 by cancer cells activates HPK1 and impairs $CD8^+$ T cell–dependent antitumor responses (Alzabin et al., 2010). Interestingly, anti-CD3–stimulated binding of GST–14-3-3ζ to GADS in vitro is reinforced by pretreating Jurkat cells with PGE2 (unpublished data). Hence, it will be interesting to address the involvement of HPK1-dependent control of microclusters in altering T cell responsiveness under pathological conditions.

In conclusion, our data demonstrate that negative feedback triggered by HPK1 plays an important role in regulating the stability of critical signaling complexes at immunological synapses. This mechanism may represent a flexible device adapting T cell responsiveness according to cell differentiation and/or external cues.

Materials and methods

Plasmids and antibodies

The pEF-FLAG-SLP76-WT expression vector was provided by G. Koretzky (University of Pennsylvania, Philadelphia, PA). pMT2-HPK1-HA and pMT2-HPK1-KD-HA plasmids (Arnold et al., 2005) were provided by F. Kiefer (Max Planck Institute for Molecular Biomedicine, Münster, Germany). HPK1-MYC and -mCherry constructs were generated by subcloning mouse HPK1 cDNA from pMT2-HPK1-HA plasmids into the pmCherry-N1 plasmid (Takara Bio Inc.) using a PCR cloning system (In-Fusion; Takara Bio Inc.). SLP76-YFP and CFP-GADS (Bunnell et al., 2006) were provided by L.E. Samelson (National Cancer Institute–Center for Cancer Research, Bethesda, MD). All point mutations were generated using the mutagenesis kit (QuikChange II; Agilent Technologies) and verified by sequencing of the entire insert cDNA. The following antibodies were used: 14-3-3ζ (C-16; Santa Cruz Biotechnology, Inc.), SLP76 (clone SLP76/03 mAb or goat polyclonal obtained from AbD Serotec and rabbit polyclonal obtained from Cell Signaling Technology), HPK1 (Cell Signaling Technology), FLAG (M2; Sigma-Aldrich), CD3 (clone UCHT1 obtained from BioLegend, MEM92 obtained

from Exbio, or HIT-3a obtained from eBioscience), CD28 (clone CD28.2; Beckman Coulter), phospho-SLP76 (Y128; clone J141-668-36-58; BD), phospho-LAT (Y191; rabbit polyclonal; Cell Signaling Technology), anti-GADS (rabbit polyclonal obtained from Millipore or mAb obtained from Santa Cruz Biotechnology, Inc.), and anti-RRXp(S/T) motif (100G7E; rabbit mAb) obtained from Cell Signaling Technology.

Cells

SLP76-deficient J14 cells (provided by A. Weiss, University of California, San Francisco, San Francisco, CA; Yablonski et al., 1998) were cultured in RPMI 1640 medium supplemented with 10% FCS and antibiotics. J14-SLP76-WT and J14-SLP76-S376A cells (Di Bartolo et al., 2007) were obtained by infecting J14 cells with pseudotyped viral particles bearing a bicistronic pMX-IRES-GFP retroviral vector coding for SLP76 constructs, either WT or S376A, respectively. Two rounds of infection were performed followed by enrichment of GFP-positive cells by fluorescence-activated cell sorting. These cells were cultured in the aforementioned medium. J14-SLP76-YFP, a cell line expressing SLP76-YFP (Lasserre et al., 2010), was generated by transfecting J14 cells with an SLP76-YFP–expressing plasmid (see Plasmids and antibodies section) by electroporation. Stably transfected cells were selected and maintained in culture medium supplemented with 1 mg/ml G418 (Invitrogen). Human $CD4^+$ T cells were isolated from peripheral blood of healthy donors using the $CD4^+$ T Cell Isolation Kit II (Miltenyi Biotec) and cultured in RPMI 1640 medium containing 10% FCS, 1 mM sodium pyruvate, nonessential amino acids, antibiotics, and 2 ng/ml IL-7 (Hung et al., 2007). Human dendritic cells were obtained by purification of monocytes from the peripheral blood of healthy donors using a $CD14^+$ cell isolation kit and 7-d culture in medium supplemented with 20 ng/ml granulocyte macrophage colony-stimulating factor and 1,000 U/ml IL4. For T cell stimulations, dendritic cells were matured using lipopolysaccharide for 24 h.

Confocal microscopy and image analysis

SLP76 and LAT microclusters were studied as previously described (Lasserre et al., 2010). In brief, cells were dropped onto glass coverslips (MatTek or LabTek) coated with anti-CD3 mAb (UCHT-1, MEM-92, or HIT-3a) or on superantigen-pulsed dendritic cells. Live cells were imaged at 37°C in RPMI 1640 medium without phenol red supplemented with 10% FCS, using a spinning-disk confocal microscope (UltraVIEW; PerkinElmer) equipped with a stage and objective heater and CO_2 incubator. Z stacks of 11 confocal sections were acquired every 5 s for 5 min or every 20 s for 20 min for stimulation with dendritic cells. Alternatively, cells were fixed at the indicated times, permeabilized, stained with the appropriate antibodies, and then analyzed by a confocal microscope (LSM700 [Carl Zeiss]; SP5 [Leica]) using a 63× oil immersion objective with a 1.4 numerical aperture. Secondary antibodies were labeled with Alexa Fluor 488 (green fluorescence channel), Cy3 (red), or Cy5 (far red). Depending on the microscope, images were acquired using Zen (Carl Zeiss), LAS AF Lite (Leica), or Volocity (PerkinElmer) software. Postacquisition treatment of images was performed using ImageJ software (National Institutes of Health).

TIRF microscopy

Cells were stimulated on anti-CD3–coated coverslips (Laboratory-Tek; Thermo Fisher Scientific), fixed, labeled, kept in PBS supplemented with 20 mM ascorbic acid (Sigma-Aldrich), and then analyzed using TIRF with an inverted microscope (IX81; Olympus).

Quantitative image analysis of microclusters and statistical analysis

A specific script for automated detection and counting of microclusters was created using the Acapella 2.0 image analysis software (PerkinElmer). For antibody-based microcluster detection, a threshold has been introduced based on the mean signal measured on unstimulated cells plated on poly-L-lysine. Microcluster lifetime was measured by analyzing videos using the Manual Tracking plug-in of the ImageJ software. Statistical data analyses were performed by the Mann–Whitney nonparametric test using Prism software (GraphPad Software).

NFAT activity assay

J14-SLP76-WT or -S376A cells were transfected with 5 µg NFAT-luciferase reporter plasmid (Mège et al., 1996) together with plasmids encoding either CFP-GADS or CFP-GADS-T254A. 10^7 cells/100 µl were electroporated using a transfection system (at 1,400 V with three pulses of 10 ms; Neon; Invitrogen). 22 h later, cells were left unstimulated or stimulated either with increasing concentrations of plate-bound anti-CD3 (6.3–100 ng/ml) plus 10 µg/ml of soluble anti-CD28 or a combination of 10 ng/ml PMA (Sigma-Aldrich) and 250 ng/ml calcium ionophore (A23187; EMD) in 96-well plates. After 5 h, cells lysis and luciferase activity assays were performed using the Cell Culture Lysis Reagent and the Luciferase Assay System (Promega) according to the manufacturer's instructions. Plates were read using a microplate luminometer (Tropix TR717; Applied Biosystems). The percentage of luciferase activity for anti-CD3/CD28-stimulated samples was calculated as follows: percent = [(RLU − MIN)/(MAX − MIN)] × 100, in which RLU is the measured luciferase activity of the sample, MIN is the mean RLU for the unstimulated sample, and MAX is the mean RLU for a sample stimulated with PMA plus Ca^{2+} ionophore.

PLA

This assay allows detection of protein–protein interactions when two antibodies coupled to complementary oligonucleotides are in sufficient proximity to allow annealing and priming of a rolling circle amplification reaction. Amplification products are then visualized by incubation with fluorescent probes. Interactions between 14-3-3ζ and potential targets were analyzed in situ by intracellular labeling with anti–14-3-3ζ rabbit polyclonal antibody combined with anti-SLP76, anti-GADS, or anti-LAT mouse mAbs followed by detection using the PLA kit (Duolink; Olink) according to the manufacturer's instructions. Fluorescence spots generated were automatically counted, and the mean number of spots per cell was calculated from nuclei counting using BlobFinder V3.2 software (Centre for Image Analysis, Uppsala University, Uppsala, Sweden).

Transient transfection and RNA interference

For transient protein expression, cells were electroporated with 5–15 µg plasmid using an electroporation device (260 V, 950 µF; Gene Pulser Xcell; Bio-Rad Laboratories), a Neon transfection system, or a Nucleofector system (Lonza). HPK1 knockdown in cell lines was obtained by electroporating 500 nM of control or HPK1-specific siRNAs (Thermo Fisher Scientific) as previously described (Lasserre et al., 2010). $CD4^+$ T cells were transfected with 1 µM siRNA using a Nucleofector system and the Human T Cell Nucleofector kit (Lonza). Cells were analyzed 72–96 h after transfection.

Cell stimulation and lysis, immunoprecipitation, and immunoblotting

Cells were stimulated by incubation at 37°C with 15 µg/ml of soluble anti-CD3 mAb (IgM, clone MEM-92). Activation was stopped by adding ice-cold PBS containing 2 mM sodium orthovanadate and 0.05% sodium azide. Cells were lysed for 10 min in ice-cold buffer containing 0.25% lauryl-β-maltoside and a cocktail of protease and phosphate inhibitors, and insoluble material was removed by centrifugation at 20,800 *g* for 10 min at 4°C. Immunoprecipitations were performed by incubating lysates for 1.5–2 h at 4°C with either anti-FLAG M2 affinity gel (Sigma-Aldrich) or protein G–coupled Sepharose beads previously coated with relevant antibodies. Beads were then washed, and bound proteins were eluted by incubating beads with a 0.2 mg/ml FLAG peptide (Sigma-Aldrich) solution or by heating them at 70°C in gel sample loading buffer. Protein electrophoresis was performed on standard SDS-PAGE or NuPAGE gels (Invitrogen). After protein electrotransfer on nitrocellulose (LI-COR Biosciences), immunoblots were saturated with blocking buffer for near-infrared fluorescent western blotting (Rockland Immunochemicals) and incubated with primary antibodies. After incubation with secondary antibodies Alexa Fluor 680 (Invitrogen), IRDye 800 (Rockland Immunochemicals), or DyLight 800 (Thermo Fisher Scientific), near-infrared fluorescence was detected and quantified by using an Odyssey scanner and the Odyssey v3.0 software (LI-COR Biosciences).

Overlay assay

Immunoprecipitated proteins were transferred onto nitrocellulose membranes that were sequentially incubated in renaturation buffer (20 mM Hepes, 50 mM NaCl, 1 mM EDTA, and 10% glycerol) containing decreasing amounts of guanidine hydrochloride (6–0.19 M). After extensive washes in renaturation buffer, membranes were saturated as described for immunoblottings and incubated overnight with 10 µg/ml GST or GST–14-3-3ζ (provided by Y.-C. Liu, La Jolla Institute for Allergy and Immunology, La Jolla, CA; Di Bartolo et al., 2007) followed by mouse anti-GST antibody and Alexa Fluor 680– or IRDye 800–coupled anti–mouse antibodies (see previous paragraph).

In vitro phosphorylation assays

WT or kinase-dead HA-tagged HPK1 was expressed in COS7 cells and purified by immunoprecipitation with an anti-HA mAb. Human GADS was subcloned into pMal C5X (New England Biolabs, Inc.), and the MBP fusion protein or MBP alone was bound on an amylose column (New England Biolabs, Inc.) and eluted with maltose according to the manufacturer's in-

structions. Equal amounts of bead-bound HPK1 constructs were mixed with 3 µg of the indicated substrate in kinase buffer (25 mM Tris, pH 7.5, 4 mM $MgCl_2$, and 1 mM $MnCl_2$) containing 5 µCi γ-[^{32}P]ATP and 20 µM of unlabeled ATP. After 30-min incubation at 30°C, the reaction was stopped by adding EDTA to a final concentration of 80 mM. Beads were then spun down, and 60% of the supernatant was spotted onto Whatman filters, which were then washed extensively with 10% TCA containing 10 mM sodium pyrophosphate and rinsed once with ethanol and then with acetone. Finally, filters were dried and radioactivity counted.

Online supplemental material

Fig. S1 shows quantification of HPK1 knockdown efficiency and effect of HPK1 knockdown or overexpression on SLP76 levels (Figs. 1 and 2). Fig. S2 shows that HPK1 knockdown or overexpression affects SLP76- but not phosphorylated LAT–containing microclusters at early stimulation time points. Fig. S3 shows that HPK1 expression and SLP76 Ser376 phosphorylation are impaired in cells transfected with HPK1 siRNA, whereas HPK1 overexpression does not affect global LAT phosphorylation. Fig. S4 shows that SLP76–14-3-3ζ complexes are specifically detected by in situ PLA but do not colocalize with SLP76 microclusters. Fig. S5 shows the effect of mutating 14-3-3 binding sites of GADS and SLP76 on phosphorylated LAT microclusters and control of GADS and SLP76 construct expression in transiently transfected cells. Video 1 shows SLP76-YFP microcluster dynamics in control versus HPK1-mCherry–overexpressing cells (Fig. 2). Video 2 shows SLP76-YFP microcluster dynamics in control cells versus cells overexpressing HPK1-KD-mCherry (Fig. 2). Video 3 shows the effect of HPK1 knockdown on SLP76-YFP microclusters induced by SEE-pulsed dendritic cells transfected with control siRNA. Video 4 shows the effect of HPK1 knockdown on SLP76-YFP microclusters induced by SEE-pulsed dendritic cells transfected with HPK1-specific siRNA. Online supplemental material is available at http://www.jcb.org/cgi/content/full/jcb.201103105/DC1.

We thank Drs. F. Kiefer, L.E. Samelson, A. Weiss, Y.-C. Liu, and G. Koretzky for kindly providing plasmids and cell lines; Dr. Mariana Mesel-Lemoine for her help in experiments with human dendritic cells; and Drs. F. Michel, S. Pellegrini, H. Soares, S. Aguera, M.I. Thoulouze, and F. Batista for critical reading of the manuscript.

This work has been funded by the Institut Pasteur, the Centre National de la Recherche Scientifique, the Agence Nationale de la Recherche, the sixth Research Framework Program of the European Union Project MUGEN (grant LSHG-CT-2005-005203), and the Israel Science Foundation. R. Lasserre has been supported by a Roux fellowship from Institut Pasteur and by the Agence Nationale de la Recherche.

Submitted: 18 March 2011
Accepted: 25 October 2011

References

Acuto, O., V. Di Bartolo, and F. Michel. 2008. Tailoring T-cell receptor signals by proximal negative feedback mechanisms. *Nat. Rev. Immunol.* 8:699–712. http://dx.doi.org/10.1038/nri2397

Alzabin, S., S. Pyarajan, H. Yee, F. Kiefer, A. Suzuki, S. Burakoff, and S. Sawasdikosol. 2010. Hematopoietic progenitor kinase 1 is a critical component of prostaglandin E2-mediated suppression of the anti-tumor immune response. *Cancer Immunol. Immunother.* 59:419–429. http://dx.doi.org/10.1007/s00262-009-0761-0

Arnold, R., I.M. Patzak, B. Neuhaus, S. Vancauwenbergh, A. Veillette, J. Van Lint, and F. Kiefer. 2005. Activation of hematopoietic progenitor kinase 1 involves relocation, autophosphorylation, and transphosphorylation by protein kinase D1. *Mol. Cell. Biol.* 25:2364–2383. http://dx.doi.org/10.1128/MCB.25.6.2364-2383.2005

Balagopalan, L., V.A. Barr, C.L. Sommers, M. Barda-Saad, A. Goyal, M.S. Isakowitz, and L.E. Samelson. 2007. c-Cbl-mediated regulation of LAT-nucleated signaling complexes. *Mol. Cell. Biol.* 27:8622–8636. http://dx.doi.org/10.1128/MCB.00467-07

Balagopalan, L., B.A. Ashwell, K.M. Bernot, I.O. Akpan, N. Quasba, V.A. Barr, and L.E. Samelson. 2011. Enhanced T-cell signaling in cells bearing linker for activation of T-cell (LAT) molecules resistant to ubiquitylation. *Proc. Natl. Acad. Sci. USA*. 108:2885–2890. http://dx.doi.org/10.1073/pnas.1007098108

Barda-Saad, M., A. Braiman, R. Titerence, S.C. Bunnell, V.A. Barr, and L.E. Samelson. 2004. Dynamic molecular interactions linking the T cell antigen receptor to the actin cytoskeleton. *Nat. Immunol.* 6:80–89. http://dx.doi.org/10.1038/ni1143

Barr, V.A., L. Balagopalan, M. Barda-Saad, R. Polishchuk, H. Boukari, S.C. Bunnell, K.M. Bernot, Y. Toda, R. Nossal, and L.E. Samelson. 2006. T-cell antigen receptor-induced signaling complexes: internalization via a cholesterol-dependent endocytic pathway. *Traffic*. 7:1143–1162. http://dx.doi.org/10.1111/j.1600-0854.2006.00464.x

Brenner, D., A. Golks, F. Kiefer, P.H. Krammer, and R. Arnold. 2005. Activation or suppression of NFkappaB by HPK1 determines sensitivity to activation-induced cell death. *EMBO J.* 24:4279–4290. http://dx.doi.org/10.1038/sj.emboj.7600894

Brill, L.M., A.R. Salomon, S.B. Ficarro, M. Mukherji, M. Stettler-Gill, and E.C. Peters. 2004. Robust phosphoproteomic profiling of tyrosine phosphorylation sites from human T cells using immobilized metal affinity chromatography and tandem mass spectrometry. *Anal. Chem.* 76:2763–2772. http://dx.doi.org/10.1021/ac035352d

Brummer, T., M. Larance, M.T. Herrera Abreu, R.J. Lyons, P. Timpson, C.H. Emmerich, E.D. Fleuren, G.M. Lehrbach, D. Schramek, M. Guilhaus, et al. 2008. Phosphorylation-dependent binding of 14-3-3 terminates signalling by the Gab2 docking protein. *EMBO J.* 27:2305–2316. http://dx.doi.org/10.1038/emboj.2008.159

Bubeck Wardenburg, J., R. Pappu, J.Y. Bu, B. Mayer, J. Chernoff, D. Straus, and A.C. Chan. 1998. Regulation of PAK activation and the T cell cytoskeleton by the linker protein SLP-76. *Immunity*. 9:607–616. http://dx.doi.org/10.1016/S1074-7613(00)80658-5

Bunnell, S.C., M. Diehn, M.B. Yaffe, P.R. Findell, L.C. Cantley, and L.J. Berg. 2000. Biochemical interactions integrating Itk with the T cell receptor-initiated signaling cascade. *J. Biol. Chem.* 275:2219–2230. http://dx.doi.org/10.1074/jbc.275.3.2219

Bunnell, S.C., D.I. Hong, J.R. Kardon, T. Yamazaki, C.J. McGlade, V.A. Barr, and L.E. Samelson. 2002. T cell receptor ligation induces the formation of dynamically regulated signaling assemblies. *J. Cell Biol.* 158:1263–1275. http://dx.doi.org/10.1083/jcb.200203043

Bunnell, S.C., A.L. Singer, D.I. Hong, B.H. Jacque, M.S. Jordan, M.C. Seminario, V.A. Barr, G.A. Koretzky, and L.E. Samelson. 2006. Persistence of cooperatively stabilized signaling clusters drives T-cell activation. *Mol. Cell. Biol.* 26:7155–7166. http://dx.doi.org/10.1128/MCB.00507-06

Campi, G., R. Varma, and M.L. Dustin. 2005. Actin and agonist MHC–peptide complex–dependent T cell receptor microclusters as scaffolds for signaling. *J. Exp. Med.* 202:1031–1036. http://dx.doi.org/10.1084/jem.20051182

Carrizosa, E., T.S. Gomez, C.M. Labno, D.A. Klos Dehring, X. Liu, B.D. Freedman, D.D. Billadeau, and J.K. Burkhardt. 2009. Hematopoietic lineage cell-specific protein 1 is recruited to the immunological synapse by IL-2-inducible T cell kinase and regulates phospholipase Cgamma1 Microcluster dynamics during T cell spreading. *J. Immunol.* 183:7352–7361. http://dx.doi.org/10.4049/jimmunol.0900973

Di Bartolo, V., B. Montagne, M. Salek, B. Jungwirth, F. Carrette, J. Fourtane, N. Sol-Foulon, F. Michel, O. Schwartz, W.D. Lehmann, and O. Acuto. 2007. A novel pathway down-modulating T cell activation involves HPK-1–dependent recruitment of 14-3-3 proteins on SLP-76. *J. Exp. Med.* 204:681–691. http://dx.doi.org/10.1084/jem.20062066

Grakoui, A., S.K. Bromley, C. Sumen, M.M. Davis, A.S. Shaw, P.M. Allen, and M.L. Dustin. 1999. The immunological synapse: a molecular machine controlling T cell activation. *Science*. 285:221–227. http://dx.doi.org/10.1126/science.285.5425.221

Hung, C.H., L. Thomas, C.E. Ruby, K.M. Atkins, N.P. Morris, Z.A. Knight, I. Scholz, E. Barklis, A.D. Weinberg, K.M. Shokat, and G. Thomas. 2007. HIV-1 Nef assembles a Src family kinase-ZAP-70/Syk-PI3K cascade to downregulate cell-surface MHC-I. *Cell Host Microbe*. 1:121–133. http://dx.doi.org/10.1016/j.chom.2007.03.004

Johnson, C., S. Crowther, M.J. Stafford, D.G. Campbell, R. Toth, and C. MacKintosh. 2010. Bioinformatic and experimental survey of 14-3-3-binding sites. *Biochem. J.* 427:69–78. http://dx.doi.org/10.1042/BJ20091834

Koretzky, G.A., F. Abtahian, and M.A. Silverman. 2006. SLP76 and SLP65: complex regulation of signalling in lymphocytes and beyond. *Nat. Rev. Immunol.* 6:67–78. http://dx.doi.org/10.1038/nri1750

Lasserre, R., S. Charrin, C. Cuche, A. Danckaert, M.I. Thoulouze, F. de Chaumont, T. Duong, N. Perrault, N. Varin-Blank, J.C. Olivo-Marin, et al. 2010. Ezrin tunes T-cell activation by controlling Dlg1 and microtubule positioning at the immunological synapse. *EMBO J.* 29:2301–2314. http://dx.doi.org/10.1038/emboj.2010.127

Liu, S.K., N. Fang, G.A. Koretzky, and C.J. McGlade. 1999. The hematopoietic-specific adaptor protein gads functions in T-cell signaling via interactions with the SLP-76 and LAT adaptors. *Curr. Biol.* 9:67–75. http://dx.doi.org/10.1016/S0960-9822(99)80017-7

Mège, D., V. Di Bartolo, V. Germain, L. Tuosto, F. Michel, and O. Acuto. 1996. Mutation of tyrosines 492/493 in the kinase domain of ZAP-70 affects multiple T-cell receptor signaling pathways. *J. Biol. Chem.* 271:32644–32652. http://dx.doi.org/10.1074/jbc.271.51.32644

Miletic, A.V., D.B. Graham, K. Sakata-Sogawa, M. Hiroshima, M.J. Hamann, S. Cemerski, T. Kloeppel, D.D. Billadeau, O. Kanagawa, M. Tokunaga, and W. Swat. 2009. Vav links the T cell antigen receptor to the actin cytoskeleton and T cell activation independently of intrinsic Guanine nucleotide exchange activity. *PLoS ONE*. 4:e6599. http://dx.doi.org/10.1371/journal.pone.0006599

Monks, C.R., B.A. Freiberg, H. Kupfer, N. Sciaky, and A. Kupfer. 1998. Three-dimensional segregation of supramolecular activation clusters in T cells. *Nature*. 395:82–86. http://dx.doi.org/10.1038/25764

Mossman, K.D., G. Campi, J.T. Groves, and M.L. Dustin. 2005. Altered TCR signaling from geometrically repatterned immunological synapses. *Science*. 310:1191–1193. http://dx.doi.org/10.1126/science.1119238

Nguyen, K., N.R. Sylvain, and S.C. Bunnell. 2008. T cell costimulation via the integrin VLA-4 inhibits the actin-dependent centralization of signaling microclusters containing the adaptor SLP-76. *Immunity*. 28:810–821. http://dx.doi.org/10.1016/j.immuni.2008.04.019

Peterson, E.J., M.L. Woods, S.A. Dmowski, G. Derimanov, M.S. Jordan, J.N. Wu, P.S. Myung, Q.H. Liu, J.T. Pribila, B.D. Freedman, et al. 2001. Coupling of the TCR to integrin activation by Slap-130/Fyb. *Science*. 293:2263–2265. http://dx.doi.org/10.1126/science.1063486

Salomon, A.R., S.B. Ficarro, L.M. Brill, A. Brinker, Q.T. Phung, C. Ericson, K. Sauer, A. Brock, D.M. Horn, P.G. Schultz, and E.C. Peters. 2003. Profiling of tyrosine phosphorylation pathways in human cells using mass spectrometry. *Proc. Natl. Acad. Sci. USA*. 100:443–448. http://dx.doi.org/10.1073/pnas.2436191100

Sauer, K., J. Liou, S.B. Singh, D. Yablonski, A. Weiss, and R.M. Perlmutter. 2001. Hematopoietic progenitor kinase 1 associates physically and functionally with the adaptor proteins B cell linker protein and SLP-76 in lymphocytes. *J. Biol. Chem.* 276:45207–45216. http://dx.doi.org/10.1074/jbc.M106811200

Shui, J.W., J.S. Boomer, J. Han, J. Xu, G.A. Dement, G. Zhou, and T.H. Tan. 2006. Hematopoietic progenitor kinase 1 negatively regulates T cell receptor signaling and T cell-mediated immune responses. *Nat. Immunol.* 8:84–91. http://dx.doi.org/10.1038/ni1416

Söderberg, O., M. Gullberg, M. Jarvius, K. Ridderstråle, K.J. Leuchowius, J. Jarvius, K. Wester, P. Hydbring, F. Bahram, L.G. Larsson, and U. Landegren. 2006. Direct observation of individual endogenous protein complexes in situ by proximity ligation. *Nat. Methods*. 3:995–1000. http://dx.doi.org/10.1038/nmeth947

Tzivion, G., and J. Avruch. 2002. 14-3-3 proteins: active cofactors in cellular regulation by serine/threonine phosphorylation. *J. Biol. Chem.* 277:3061–3064. http://dx.doi.org/10.1074/jbc.R100059200

Vardhana, S., K. Choudhuri, R. Varma, and M.L. Dustin. 2010. Essential role of ubiquitin and TSG101 protein in formation and function of the central supramolecular activation cluster. *Immunity*. 32:531–540. http://dx.doi.org/10.1016/j.immuni.2010.04.005

Varma, R., G. Campi, T. Yokosuka, T. Saito, and M.L. Dustin. 2006. T cell receptor-proximal signals are sustained in peripheral microclusters and terminated in the central supramolecular activation cluster. *Immunity*. 25:117–127. http://dx.doi.org/10.1016/j.immuni.2006.04.010

Wang, H., B. Wei, G. Bismuth, and C.E. Rudd. 2009. SLP-76-ADAP adaptor module regulates LFA-1 mediated costimulation and T cell motility. *Proc. Natl. Acad. Sci. USA*. 106:12436–12441. http://dx.doi.org/10.1073/pnas.0900510106

Yablonski, D., M.R. Kuhne, T. Kadlecek, and A. Weiss. 1998. Uncoupling of nonreceptor tyrosine kinases from PLC-γ1 in an SLP-76-deficient T cell. *Science*. 281:413–416. http://dx.doi.org/10.1126/science.281.5375.413

Yokosuka, T., K. Sakata-Sogawa, W. Kobayashi, M. Hiroshima, A. Hashimoto-Tane, M. Tokunaga, M.L. Dustin, and T. Saito. 2005. Newly generated T cell receptor microclusters initiate and sustain T cell activation by recruitment of Zap70 and SLP-76. *Nat. Immunol.* 6:1253–1262. http://dx.doi.org/10.1038/ni1272